BOLETIN DE LA SOCIEDAD ESPAÑOLA DE
Cerámica y Vidrio
www.elsevier.es/bsecv

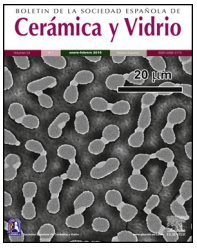

Fabrication, characterization, and *in vitro* evaluation of β-TCP/ZrO_2-phosphate-based bioactive glass scaffolds for bone repair

Criseida Ruiz-Aguilar[a,*], *Luz Eugenia Alcántara-Quintana*[b], *Ena Athenea Aguilar-Reyes*[c], *U. Olivares-Pinto*[a]

[a] *Escuela Nacional de Estudios Superiores Unidad Juriquilla, Universidad Nacional Autónoma de México, Campus UNAM-Juriquilla, Boulevard Juriquilla 3001, CP 76230 Santiago de Querétaro, Qro, Mexico*
[b] *Catedra CONACyT. Facultad de Enfermería y Nutrición, Universidad Autónoma de San Luis Potosí, Av. Niño Artillero 130 Zona Universitaria, 78240 San Luis Potosí, Mexico*
[c] *Instituto de Investigación en Metalurgia y Materiales, Universidad Michoacana de San Nicolás de Hidalgo, Av. Francisco J. Múgica S/N, CP 58030 Morelia, Mich., Mexico*

ARTICLE INFO

Article history:
Received 16 April 2020
Accepted 3 September 2020
Available online 5 October 2020

Keywords:
Calcium phosphate
Bioactive glass
Scaffold
Zirconia
Hydroxyapatite

ABSTRACT

Scaffolds have proven to be an excellent option for the regeneration of bone tissues; since they present excellent results of architecture, composition, and functionality. Therefore, scaffolds can be used as implants to repair bones and show guided regeneration, allowing complete restructuring of damaged tissue, as well as allowing the site where the implant is located to have functionality. In the present investigation, three different beta-phase tricalcium phosphate/zirconia-reinforced phosphate-based bioactive glass compositions were evaluated: V1, VZ0.5, and VZ1.0 (0, 0.5, and 1 mol%). All scaffolds showed excellent bioactivity and osteoconductivity results. They were forming HA crystalline aggregates with the typical cauliflower morphology *in vitro* studies in simulated body fluid and with human osteoblasts (MG-63).

On the other hand, cell proliferation analyzed using the BrdU assay and apoptosis using Annexin V. As well as the viability (MTT assay) and adhesion (RT-PCR of beta 3 integrin) of osteoblasts at day 14. Zirconia had a significant positive effect on cell proliferation as well as in the cell adhesion, with a substantial proliferation for the scaffold with VZ1.0 composition. Due to the zirconia modifies the scaffold surface, allowing greater cell adhesion, an essential step for cell proliferation to take place.

* *Corresponding author.*
E-mail address: criseida@unam.mx (C. Ruiz-Aguilar).
https://doi.org/10.1016/j.bsecv.2020.09.004

Fabricación, caracterización y evaluación *in vitro* de andamios de β-TCP/ZrO_2-vidrio bioactivo a base de fosfato para la reparación ósea

Palabras clave:
Fosfato de calcio
Vidrio bioactivo
Andamio
Zirconia
Hidroxiapatita

RESUMEN

Los andamios han mostrado ser una excelente opción para la regeneración de los tejidos óseos, ya que presentan excelentes resultados de arquitectura, composición y funcionalidad. Por lo tanto, los andamios pueden ser empleados como implantes para reparar huesos y mostrar regeneración guiada, permitiendo la reestructuración completa del tejido dañado, así como permiten que el sitio en donde se encuentra el implante tenga funcionalidad. En la presente investigación, se evaluaron tres diferentes composiciones de fosfato tricálcico fase beta/vidrio bioactivo base fosfato reforzado con zirconia: V1, VZ0.5, y VZ1.0 (0, 0,5 y 1 mol%). Todos los andamios mostraron excelentes resultados de bioactividad y de osteoconductividad. Se observó la formación de agregados cristalinos de la fase HA con la típica morfología coliflor en los estudios *in vitro* de los andamios sumergidos en fluido corporal simulado y con osteoblastos humanos (MG-63). Por otro lado, se analizó la proliferación celular mediante ensayo de BrdU, y apoptosis mediante anexina V. Así como la viabilidad (ensayo de MTT) y la adhesión (RT-PCR de integrina beta 3) de los osteoblastos al día 14. La zirconia tuvo un efecto positivo significativo en la proliferación celular, así como en la adhesión celular para el andamio con la composición VZ1.0, debido a que la zirconia modificó la superficie del andamio, permitiendo una mayor adhesión celular, paso importante para que se pueda llevar a cabo la proliferación celular.

Introduction

Scaffolds have suitable characteristics to be used in tissue engineering to repair and restore bone tissue. One of the most important is interconnected porosity that is essential for cell nutrition, cell proliferation, and the migration of bone cells through the scaffolds [1–3]. Other important scaffold properties are biocompatibility, osteoconductivity, controlled degradation, mechanical properties, and formability [4–7]. Materials with a composition close to that of natural bone, such as hydroxyapatite (HA) and tricalcium phosphate (TCP), especially the beta phase (β-TCP), possess those characteristics [8], but its low level of mechanical properties and high solubility have limited β-TCP use in medical applications [9]. On the other hand, phosphate-based bioactive glasses have showed a favorable response in biological environments because they are free of silica, resulting in better biocompatibility in biological tissues [10,11]. Furthermore, the addition of metal oxides, such as MgO, TiO_2, ZrO_2, Al_2O_3, and Li_2O, into glass composition can enhance their physicochemical properties of osteoconductivity and compressive strength and reduce degradation activity [12,13]. The mechanical properties and bioactivity of bioglasses have been favorably influenced by the addition of ZrO_2, due to its capacity to decrease their solubility [14]. The combination of calcium phosphates (HA and TCP) and bioactive glasses (silica- and phosphate-based glasses) improved their biological properties and the composites showed a faster bioactive response than the use of bioglass and HA, separately [15]. However, it is important to note that dissolution depends on other factors, such as porosity, pore shape, pore size, and pore interconnectivity in the samples [16].

Five different scaffolds compositions were physically, chemically, and structurally characterized in a previous investigation [17]. Where, V1, VZ0.5, and VZ1.0 were the best three scaffolds composition, which showed pore size, porosity, and mechanical properties adequate for bone tissue applications. The three compositions referred before are the samples evaluated *in vitro* in the present work, complementing the information of the scaffolds in cell culture and in simulated body fluid.

The main objective of our research was to evaluate the *in vitro* bioactivity and human osteoblast viability of TCP/phosphate-based bioglass scaffolds containing 0, 0.5, and 1 mol.% of ZrO_2. The morphological and structural characterization of various compositions of doped scaffolds with varying amounts of zirconia (0, 0.25, 0.5, 0.75, and 1.0 mol.%) were reported in a previous analysis [18], and the samples whose compositions contained 0.5 and 1.0 mol % of zirconia had better results in terms of interconnected porosity, compressive strength (0.6–1 MPa), porosity (51–53%), and pore size distribution (1.41–303 mm).

Materials and methods

Scaffold fabrication

Phosphate-based bioglass with the composition of $45P_2O_5$–30CaO–(25–x) Na_2O–xZrO_2 was produced in the laboratory by melt-quenching technique. It was doped with ZrO_2 IV (Sigma–Aldrich, 99%) in various amounts: 0, 0.5, and 1.0 mol.%. The combined method of powder technology and foaming of polymers was used for scaffold fabrication in this research [19]. The scaffolds were performed used

β-tricalcium phosphate (Sigma–Aldrich, >95%) and bioglass. Powders relation was 55 wt.% (80 wt.% of β-TCP/20 wt.% of bioglass). The 45 wt.% powders remaining were distributed in 2.5 wt.% of p-toluene sulfonyl hydrazide (TSH) (foaming agent, Sigma–Aldrich 97%) and 42.5 wt.% of phenolic resin (binder). The mixture was homogenized on a conventional ball mill for 30 min and compressed into a stainless-steel mold. The thermal process was carried out in three stages: foaming, pyrolysis, and sintering. During foaming, the binder was melted and a suspension of phosphate-based bioglass/β-TCP particles was produced. At this same stage, the foaming agent also decomposed and released a gas that expanded the structure, which allowed the formation of interconnected porosity throughout the scaffold. At the second stage, the burn-out of the polymer was performed at an intermediate temperature (500 °C), and at the third stage, the sintering of the scaffold at 980 °C for 1 h provided mechanical strength by the necking between particles.

Bioactivity assays

In vitro bioactivity studies were conducted to examine the ability of the scaffolds to form hydroxyapatite. SBF solution was prepared in the laboratory, following the protocol proposed by Kokubo et al. [20], using polyethylene containers, high purity chemical reagents from Sigma-Aldrich, and deionized water. The SBF was stored at 4 °C for 24 h to determine the presence of precipitates. Each scaffold (V1, VZ0.5, and VZ1.0, the nomenclature used for scaffolds containing 0, 0.5, and 1 wt.% of ZrO_2, respectively) was placed in a conic vial with 15 mL of SBF solution for varying immersion times: 7, 14, 21, and 28 days in static conditions. The scaffolds were then washed with distilled water, dried in a furnace at 100 °C for 12 h, and kept in a desiccator for further characterization. The variation of pH in the SBF was measured in all samples every three days, for 28 days, using a pH-meter (Thermo Onion, USA Model-720A).

For the calculation of the SBF volume was necessary to consider the porosity of the scaffold. The radius of the scaffolds was 5 mm and a height of 20 mm. Therefore, the surface area of each scaffold was 157.07 mm^2, and the volume was calculated according to the empirical equation: $V_s = S_a/10$, where denominator 10 allowed direct conversion of units from mm^2 to mL [21]. The variable V_s corresponded to the volume in mL of the SBF solution. The S_a variable was the apparent surface area of the specimen in mm^2. The volume calculated obtained in the previous equation was 15.70 ml. However, the scaffolds absorbed part of the SBF, decreasing the volume. Thus, it considered that the initially calculated volume was multiplied by a factor of 1.28, allowing a better interaction of the SBF solution with the scaffolds, obtaining a total volume of 20.09 ml for each sample.

Mass spectrometer by inductively coupled plasma (ICP-MS)

The equipment used to carry out the analyzes of Inductively coupled plasma mass spectrometry (ICP-MS) was the Spectro Analytical Instruments Aligent, model 7500c, a micromole of SBF sample was used as a control to analyze the amount in ppm of Zr, in addition to of the elements Ca and P.

Cell culture

The MG-63 (ATCC CRL-142) osteoblasts cells were maintained in growth medium α-MEM (Gibco, Thermo Fisher, Massachusetts, MA, USA) with 10% Fetal Bovine Serum (Gibco, Thermo Fisher) and 1% antibiotics. The cells were harvested at confluence with trypsin/EDTA (Gibco, Thermo Fisher) and transferred into cell culture flasks and maintained at 37 °C in humidified atmosphere of 5% CO_2 and 95% air.

The MG-63, ATCC CRL-142 osteoblasts cells ($5X10^4$ cell/well) were cultured in 96-well plates (Costar, Thermo Fisher) for 14 days at 37 °C, 5% CO_2 and 95% air. The cells were placed on the scaffolding V1, VZ0.5, VZ1.0.

Cell viability assay

After incubation for 14 days, 100 μL of 3-(4,5-dimethylthiazol-2-yl)-2,5-diphenyl tetrazolium bromide (MTT, 5.0 mg/mL) was added to each well. After 4 h, the formazan product was dissolved in dimethyl sulphoxide and the absorbance at 570 nm was measured using a microplate reader. Non-treated cells were used as negative.

Apoptosis analysis

Apoptotic cells were measures using Annexin V-FITC (475 nm) Apoptosis Staining/Detection Kit according to the manufacturer's instructions. Briefly, cells were washed once with PBS 1×, and centrifugated at 13,000 rpm for 5 min. After that, were washed once in 1× binding buffer and resuspended in 1× staining buffer to 10^6–10^7 cells/ml. Then, 100 μl (about 5×10^5 cells) were incubated with 10 ul de Annexin V- at room temperature for 15 min in the dark. Finally, annexin V stained cells were analyzed with confocal microscopy as a measure of cell apoptosis. The staining of treated cell lines and experiments were repeated three times.

Cell proliferation assay

The cells were incubated on glass coverslips in a Petri dish at 37 °C in a humidified atmosphere containing 5% CO_2 with or without 10 μM BrdU, for 20 min or 1 h. After 10-min fixation with 2% formaldehyde and permeabilization in 0.1% Triton X-100 in PBS, the incorporated BrdU was revealed using fluorescence Anti-BrdU antibody, [BU1/75 (ICR1)].

Real-time PCR

On day 14, cells cultured on V1, VZ0.5, VZ1.0 submitted to total RNA extraction with Trizol reagent (Invitrogen) following the manufacturer's instructions. An equal amount of each sample (1 μg) was used for reverse transcription reaction (Kit High Capacity, Invitrogen-Life Technologies). Real-time PCR was performed in a Step One Plus Real-Time PCR (Thermo Fischer Scientific) with TaqMan® PCR Master Mix (Applied Biosystems, Foster City, CA, USA). The reactions were done in triplicates ($n = 3$), using 5 μL of TaqMan® Gene Expression

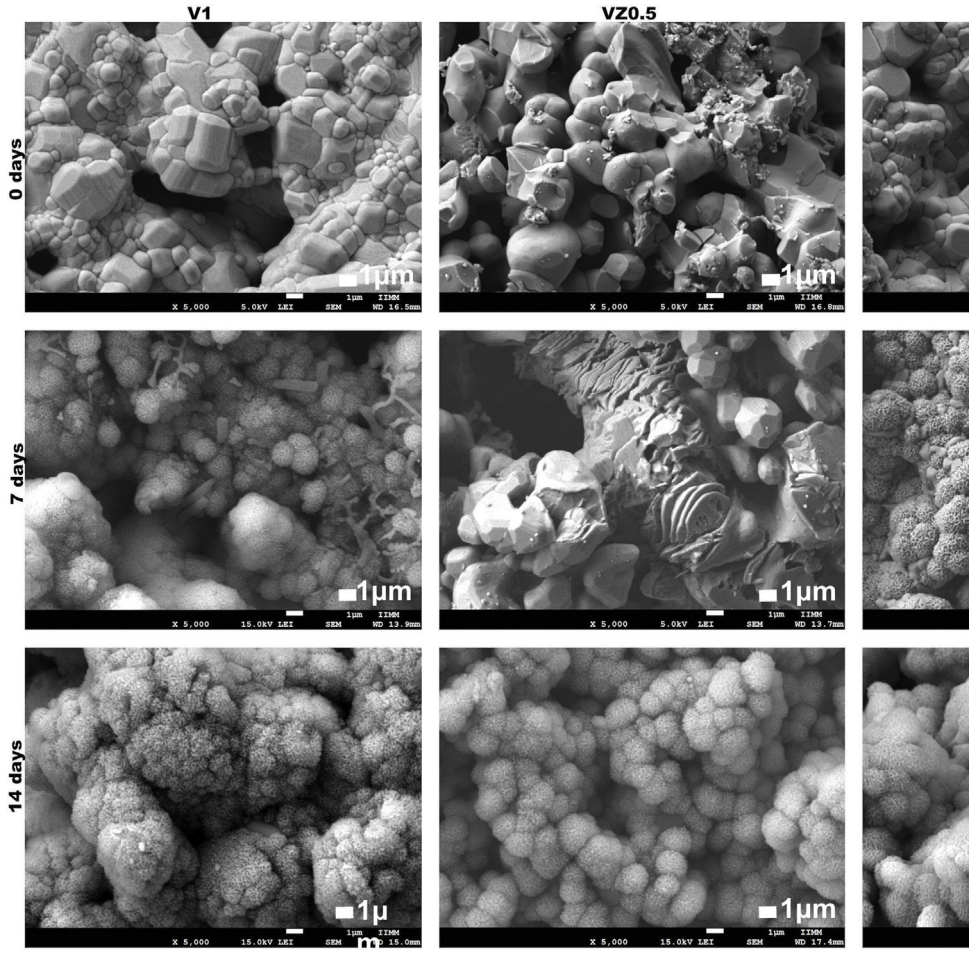

Fig. 1 – FESEM micrographs of the V1, VZ0.5, and VZ1.0 scaffolds before immersion and after 7 and 14 days of immersion in SBF.

Master Mix, 0.5 µL of TaqMan® probes and 4.5 µL of cDNA (11.25 ng). The relative integrin β3 gene expression in was normalized to β-actin expression and the changes were relative to the expression of cells.

Fourier-transform infrared spectroscopy Characterization

Infrared analyses were performed in a Bruker Tensor 27 FTIR Spectrometer to determine the functional groups present on the scaffold, before and after immersion in SBF. For this purpose, tablets of 1 mm in thickness and 1.3 cm in diameter were prepared with 0.003 g of the sample and 0.3 g of KBr, and the data were collected in a range of 4000–400 cm^{-1}. The scaffolds were analyzed through X-ray diffraction to identify the crystalline phases, before and after immersion in SBF, and to confirm the formation of hydroxyapatite. The D8 Advance Bruker X-ray Diffractometer was used with CuKα radiation in the 2-theta range of 10–80° with 16 s/step. A Field Emission Scanning Electron Microscope (FESEM JEOL JSM-7600F) was used to analyze the microstructure of sintered scaffolds, before and after immersion in SBF. Additionally, EDS was used to determine the Ca/P ratio present on the surface of the scaffolds after immersion in SBF and the reported value was the average of 5 measurements. The adhesion of MC3T3-E1 subcloned 4 cells on the scaffolds was also analyzed by SEM after 3 days. The preparation of samples included the dehydration of the material, which was performed by immersing the samples at various concentrations of ethanol solutions (mixture of absolute ethanol with PBS) for 10 min each: 25, 50, 75, and 98%, respectively. The immersion at 98% was done twice. The samples were dried in a laminar flow hood for at least 12 h. Finally, each scaffold was sealed with parafilm and stored at −20 °C.

Micro-Raman characterization

The micro-Raman measurements performed on a Thermo Scientific DXR spectrometer. The line laser wavelength excitation was 532 nm. The microscope objective was used at 50 × with a laser power of 20 mW for the sample. Spectra recorded at room temperature within a 3572–35 cm^{-1} range.

Results

Fig. 1 shows the FESEM images of the porous scaffolds, before and after immersion in SBF. In the as-sintered scaffolds, the

variation of pore size can be observed, as well as the good interconnection between the pores and their necks. The samples formed hydroxyapatite (HA) precipitates on the surface at 7 days of immersion in SBF and the growth of the HA layer continued up to days 14 and 21. The HA almost completely covered the surface with a cauliflower-like morphology. A slower HA formation rate was observed in the VZ0.5 scaffold than the V1 and VZ1.0 compositions. The HA behavior in the VZ0.5 sample was attributed to the manipulation before it was observed by FESEM. Nevertheless, at 14 days all the compositions showed a total coverage of HA on the surface of the scaffolds. The images took at 21 days did not show a significative variation of HA formation in comparison of the samples submerged in SBF after 14 days. The role of zirconia in the scaffolds was essential to enhance their bioactivity, observing with more clarity in all the samples from 14 days.

Fig. 2 shows the FTIR spectrum for the as-sintered VZ1.0 scaffolds, before immersion in SBF. The presence of phosphate groups at 561 and 606 cm^{-1} corresponded to the stretching modes for PO_4 [23–27] At 720 cm^{-1}, a functional group related to calcium pyrophosphate (P_2O_7) was found [22,26,27]. Phosphate groups of the υ_1 type were located at 974 cm^{-1} and υ_3 PO_4 groups were located at 1006, 1025, 1100, and 1213 cm^{-1} [24,25,27,29]. It should be mentioned that the principal functional phosphate groups of the β-TCP were located at the 1100, 1006, and 974 cm^{-1} wavelengths, as reported by other authors [24,29].

The FTIR spectra for the VZ1.0 scaffolds at various SBF immersion times (7, 14, 21, and 28 days) are also shown in Fig. 2. Peak transmittance bands at 570 and 962 cm^{-1} correspond to the phosphate groups in the β-TCP phase, related to the υ_4 and υ_1 vibrational modes, respectively [22,23,25,29–32]. The same pyrophosphate as previously observed in the FTIR of the scaffold, before being immersed in SBF, was observed at 720 cm^{-1} [26–29]. On the other hand, the characteristic FTIR chemical groups for the hydroxyapatite phase were PO_4^{3-}, OH^-, and CO_3^{2-}. The peaks found at 1420 and 1650 cm^{-1} were characteristic bands of carbonate functional groups (CO_3^{2-}) for the υ_3 and υ_4 vibrational modes [23,25,27,33] and OH^{-1} groups at 2250, 2890, and 3432 cm^{-1} [23,26,30,34]. Oliveira et al. [35] reported of the formation of a hydroxyapatite layer on scaffolds after 7 days of immersion in SBF, showing variations in wavelength at 3400 cm^{-1}, as a consequence of water molecules incorporated in hydroxyapatite, due to apatite has a hygroscopic nature, it means, HA contains chemically bound water in its structure also known as structural water.

The main changes in the samples after immersion in SBF were the elimination of several peaks corresponding to the phosphate groups at 606 cm^{-1}, related to the υ_4 PO_4, in addition to the peaks at 1006, 1025, and 1100 cm^{-1}, corresponding to the υ_3 phosphate groups, and the appearance of new functional groups, such as the carbonate groups (CO_3^{2-}), with two different vibration modes (υ_3 and υ_4), and the OH^- groups, as a result of the hydroxyapatite phase formation.

However, the scaffolds revealed the content of type B carbonate, which replaced the phosphate groups at 7 and 14 days. On the other hand, the supersaturation of calcium and phosphate ions from the SBF solution and the scaffolds caused a greater dissolution effect of the HA layer, as a consequence of the static conditions, occasioning in a decrease of the carbonate peak, exhibiting an imbalance between the layer of HA formed and the layer in process of formation.

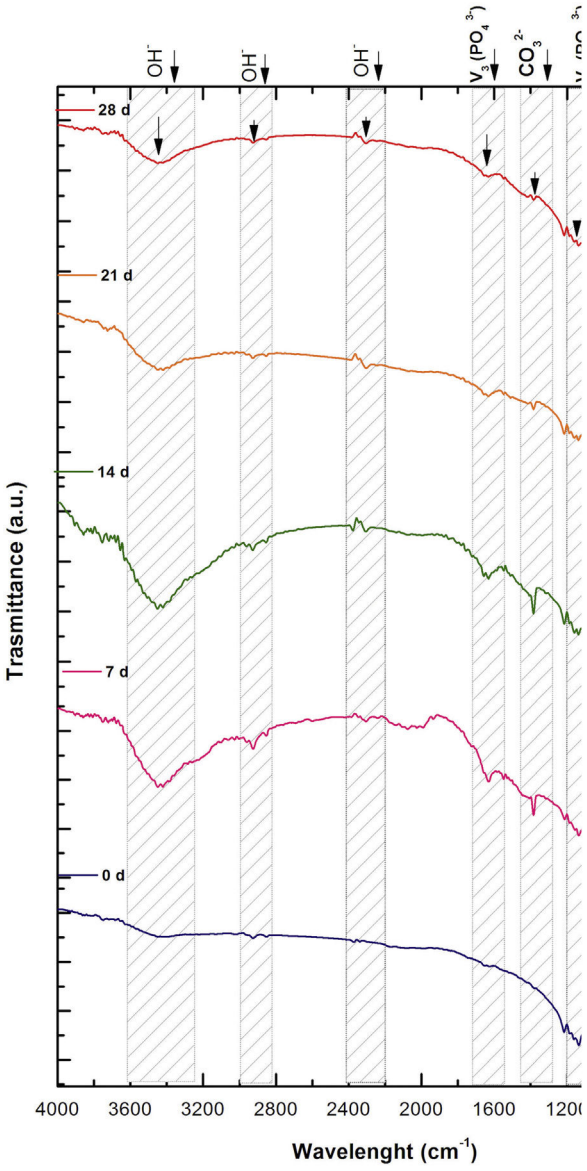

Fig. 2 – FTIR spectra showing the main functional groups of the VZ1.0 scaffolds before and after various immersion times in SBF.

The FTIR spectra showed that as the immersion time in SBF increased, the characteristic signals of the carbonate and OH^- groups grew. However, the phosphate group peaks decreased at a range of 1000 and 1100 cm^{-1}. These results corroborate the presence of the hydroxyapatite phase observed in the SEM images. Fig. 3 offers a better view of the phosphate groups partially replaced by the carbonate groups in the crystal structure.

The three predominant crystalline phases identified for the V1 scaffold before SBF immersion were: $Ca_3(PO_4)_2$, (JCPDS 01-073-4869), $Ca_2P_2O_7$ (JCPDS 01-071-2123), and Na_3PO_4 (JCPDS

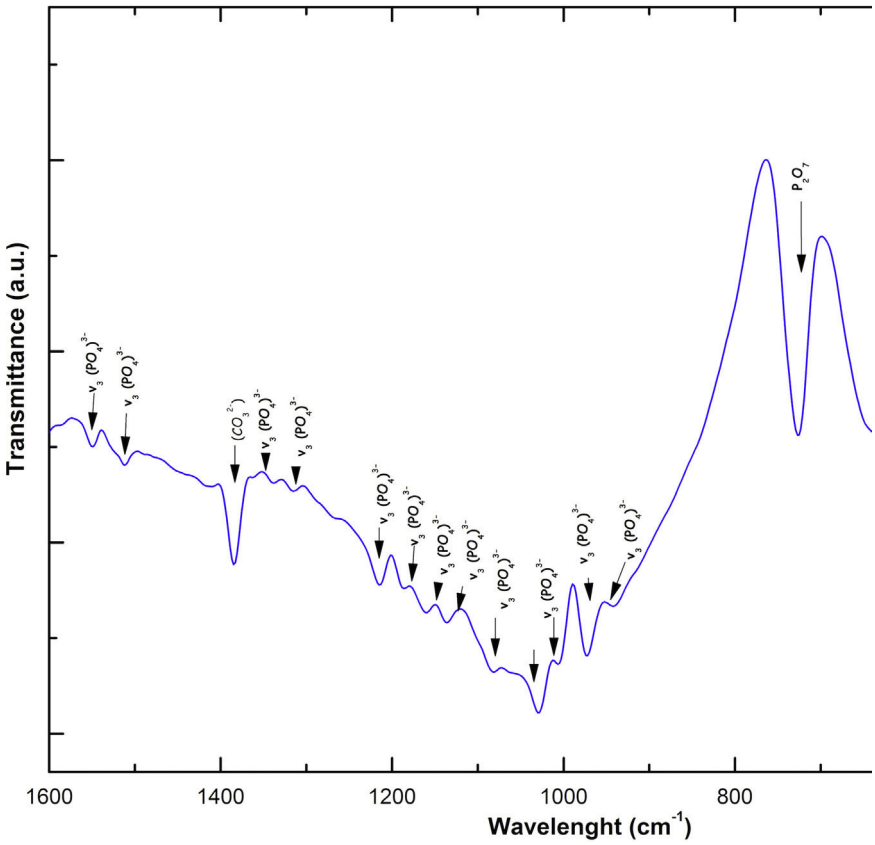

Fig. 3 – FTIR spectrum showing absorption bands of the VZ1.0 scaffold after 28 days of immersion in SBF.

01-076-0201). The VZ0.5 and VZ1.0 scaffolds presented two additional phases: $CaZrO_3$, (JCPDS 01-072-7552) and ZrP_2O_7 (JCPDS 00-024-1490). After 7 days of SBF immersion, the scaffolds formed the new crystalline phase, hydroxyapatite $Ca_{10}(PO_4)_6(OH)_2$ (JCPDS 01-071-2123), as showed in Fig. 4, along with the beta tricalcium phosphate $Ca_3(PO_4)_2$ and Na_3PO_4 major phases and the $CaZrO_3$ and ZrP_2O_7 minor phases. The two phases $CaZrO_3$ and ZrP_2O_7 were results of the substitution of zirconium in the structure of tricalcium phosphate and phosphate-based glass. Rajkumar et al. [10] studied the effect of zirconia on the internal structure of phosphate-based glass after SBF, where they reported that zirconia caused anomalous behavior in the network of the glass structure, that is, at amounts less than 0.5 mol.% of zirconia, causing a decrease in density. However, from 0.5 and 1.0 mol.% of zirconia, the samples presented an increase in its density, promoting an inverse relationship between the zirconia content and the molar volume.

The pH measures at 7, 14, 21 and 28 days were made in all the samples dipped in SBF. Showing a pH increase close to 8 at 7-day. Nevertheless, at 14, 21 and 28 days, the samples were stabilized between 7.6 and 7.7, allowing the HA formation on the surface of the scaffolds as Fig. 5 illustrates. After the scaffolds immersed in SBF, it was observed that the calcium pyrophosphate phase was dissolved entirely due to the lack of thermodynamic stability as it has a Ca/P ratio equal to 1. Reason why the interaction of PO_4^{3-} ions acidified the environment of the SBF, provoking the dissolution of the scaffold, but at the same time, the Ca^{2+} ions alkalinize the SBF medium. These two phenomenons generated that the thermodynamic driving force involved in HA precipitation on the scaffolds occurred due to nuclei formation on the surface of the scaffold being the pH is a determining parameter. When the pH is at values above 7.4 and less than 10, in addition to the presence of carbonate ions, HA is more stable and kinetically favors precipitation [36]. On the other hand, the effect of zirconium decreases the dissolution effect on scaffolds, increased surface roughness, and the hydroxyapatite formation [17].

The scaffolds V1, VZ0.5, and VZ1.0 indicated dissolution in the SBF solution of the calcium and phosphorus elements, and zirconium was contained in the samples VZ0.5 and VZ1.0. On the other hand, the V1 scaffold presented a bimodal tendency of the values of calcium and phosphorus ions, as a result of degradation uncontrolled of the sample, exhibiting a pH variation in the simulated body fluid, besides the static condition of the bioactivity test could have affected to pH results. Nevertheless, the Zr helped to stabilize the calcium and phosphorus ions in the samples VZ0.5 and VZ1.0 as Fig. 6 shows.

Fig. 7 shows the Raman results obtained from the V1 scaffolds after being evaluated in vitro in SBF. The mode υ_2 vibration corresponds to PO_4 type symmetric links presented in the range of 389–450 cm^{-1}; this group is the result of the

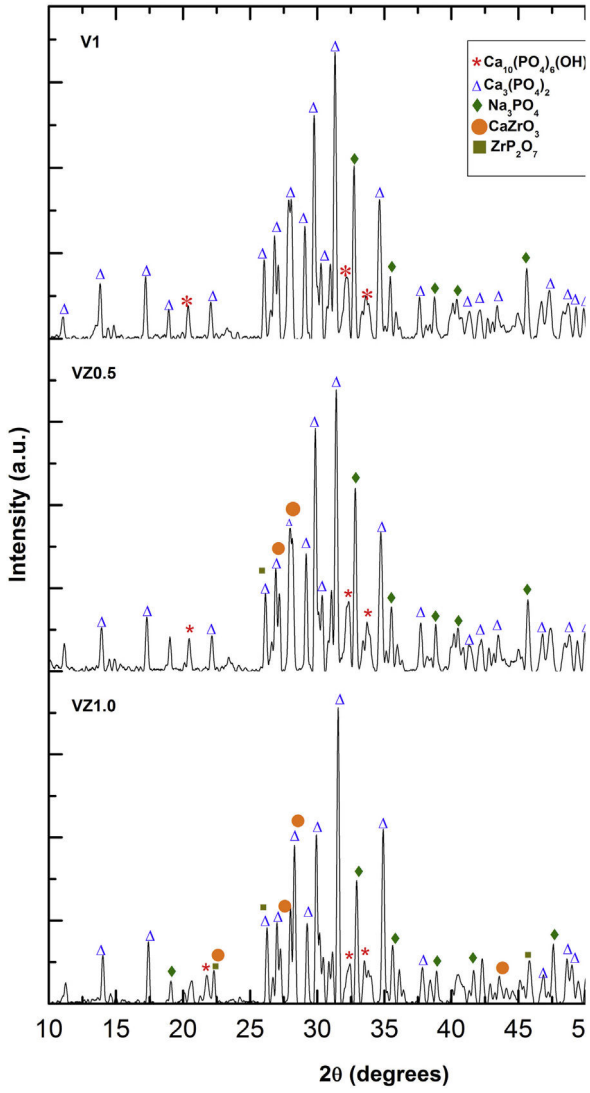

Fig. 4 – XRD patterns for the V1, VZ0.5, and VZ1.0 scaffolds immersed in SBF for 7 days.

composition of the scaffolds from both β-TCP and the bioactive calcium phosphate-based glass. The υ_4 vibration mode matches to links of the PO_4 type of asymmetric type (O—P—O) in the range of 600–680 cm^{-1}. In addition to a peak found at a wavelength of 735 cm^{-1} corresponding to a pyrophosphate (CaP_2O_7) [37]. Calcium pyrophosphate phase decreased at longer exposure times in SBF as a consequence of solubility kinetics, where the microporosity of the scaffolds was a decisive biodegradation factor [38].

On the other hand, the presence of the υ_1 vibration mode was observed in the wavelength range of 900–1000 cm^{-1}, representing P—O type symmetric bonds in a characteristic double band of the β-TCP compound. This crystalline phase was part of the scaffold compositions, which showed a significant increase at 7 and 14 days after the scaffolds submerged in SBF. This change was as a consequence of the ionic interaction of PO_4^{3-} and Ca^{2+} ions. Similarly, an intense peak was found at 1073 cm^{-1} before the scaffolds evaluated in SBF. Which corresponds to the asymmetric stretching vibration υ_3 mode (P—O), however, at 7 and 14 days it was observed that there was a significant decrease in the peak due to the substitution of carbonate A and B type, mostly of type B. Due to the carbonate ion type υ_1 substitutes phosphate sites, forming of carbonated hydroxyapatite in the scaffolds. The peaks presented in the range from 1050 to 1180 cm^{-1} correspond to the υ_3 vibration mode of the functional group P—O [39–42].

On the other hand, Fig. 8a and b shows the two scaffolds VZ0.5 and VZ1.0 with a splicing of functional groups in the peak presented at 745 cm^{-1}. The first corresponds to the crystalline phase of calcium pyrophosphate and the second to the vibration mode υ_4 matching to the group asymmetric type PO_4 phosphate (O—P—O). CaP_2O_7 presented the physicochemical phenomenon of dissolution at the longest exposure time in SBF. However, the peak consistent with the υ_4 vibration mode phosphate ions increases due to the incorporation of carbonate ions of type B.

The peaks of the vibration mode of the υ_3 type phosphates shown in the range of 1050–1180 cm^{-1}, increases the intensity due to the presence of the carbonate groups as a consequence of the formation of carbonated hydroxyapatite [39]. The VZ1.0 sample presented more significant bioactivity after 7 days result of the incorporation of CO_3^{2-} ions, increasing the intensity of the peak corresponding to the υ_3 vibration mode, followed by the VZ0.5 sample with a lower intensity at that of the VZ1.0 scaffolds and finally the V1 sample.

Fig. 9 shows us in (a) cell viability, in (b) percentage of cells in proliferation, and in (c) the percentage of apoptotic cells. In (a), MTT results showed that activity metabolism of osteoblasts increased on day 14 with a significant difference in the VZ1.0 biomaterial. These results also indicate that osteoblasts remain viable on biomaterial treasures until day 14. In (b), the BrdU antibody binds to the cells in the synthesis phase, what the results tell us is that the VZ1.0 biomaterial had a better effect on the proliferation of osteoblasts, indicating that it is a better surface for cell proliferation. Similarly, in the case of annexin V, which is a protein that binds phosphatidylserine and indicates the formation of apoptotic bodies, or programmed cell death. The results indicate that the VZ1.0 biomaterial is the best, since it induces less apoptosis in a significant way.

Fig. 10 shows the relative gene expression of β3 integrin, this protein is of cellular adhesion and its participation in the differentiation of osteoblasts has been described. So, in this sense, the VZ1.0 scaffold is the one that presents a significantly higher adhesion.

Discussion

The interconnected macroporous structure is considered essential for the growth of new bone tissue, which provides an environment of high ionic strength, in which fluids are bone cell carriers. The range of pore size in the scaffolds was 1.41–303 mm, which resulted from the sintering between the bioglass necks and the β-TCP particles, as reported in a previous investigation [17]. No significant relation was found

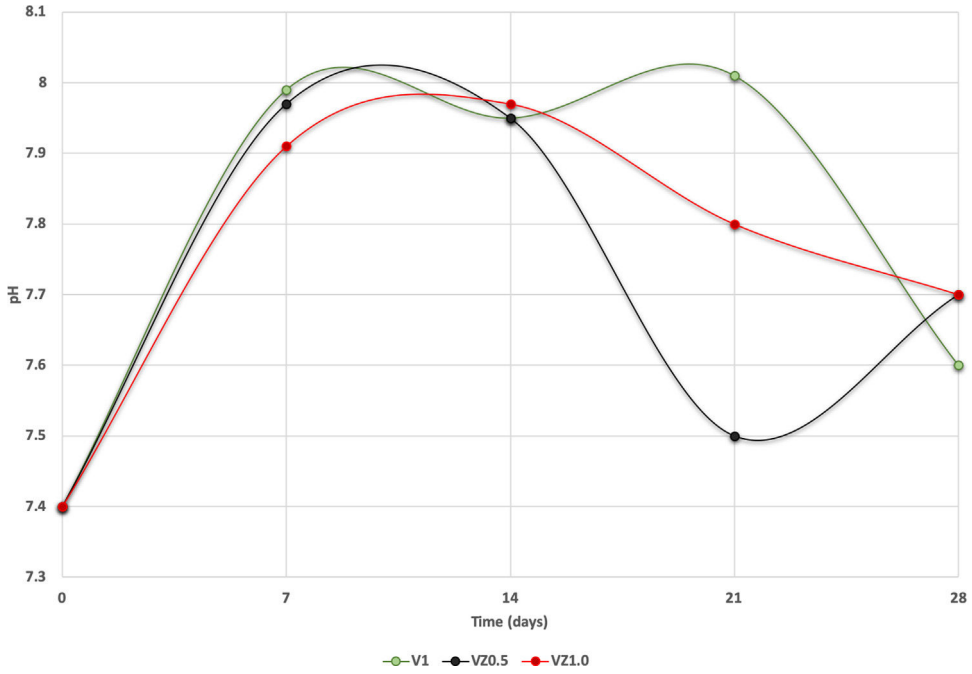

Fig. 5 – pH variation as a function of immersion time in SBF solution in the different compositions of the scaffolds.

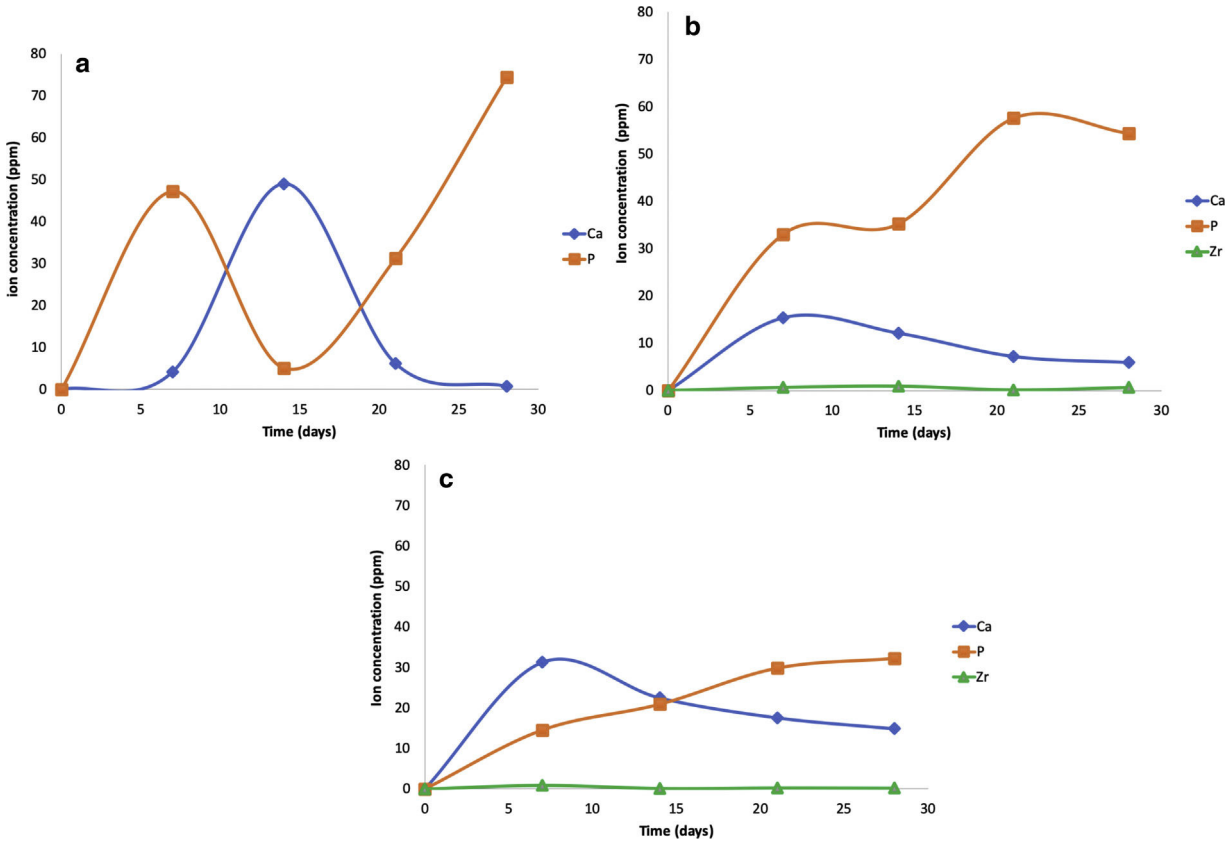

Fig. 6 – Ca, P and Zr ions concentrations of the samples (a) V1, (b) VZ0.5 and (c) VZ1.0 before they were dipping in SBF solution at different times (7, 14, 21 and 28 days).

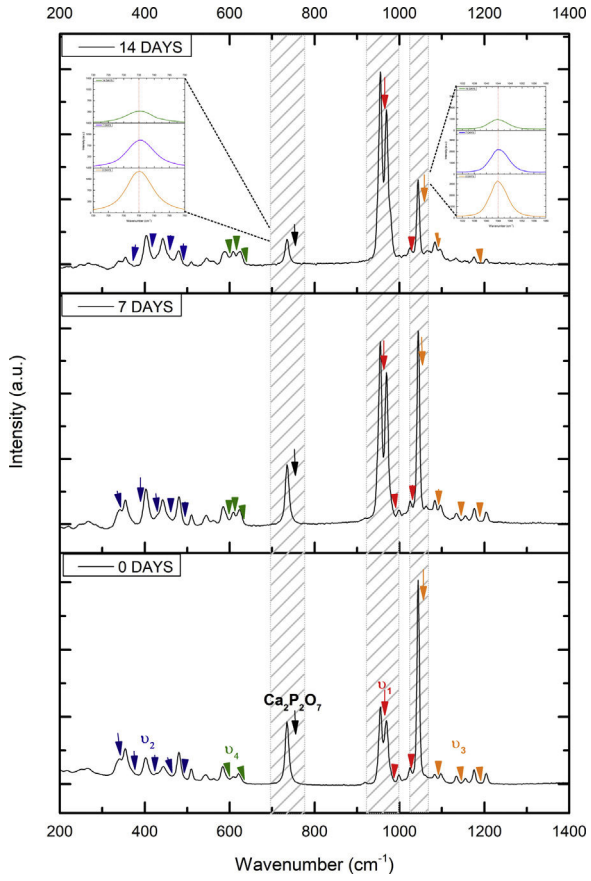

Fig. 7 – Raman spectrum of sample V1 shows the main groups found after being immersed in SBF at different days (7 and 14 days).

with respect to pore size and fixation force. Kenapfel et al. [34] observed that the effect of pore size in the scaffolds was crucial for adequate attachment. They carried out studies verifying that information in canine animal models, in which pore sizes were as small as 50 μm and as large as 800 μm and found that pore sizes smaller than 100 μm increased the attachment force. Furthermore, Mastrogiacomo et al. [43] concluded that bioceramics made from a porous cellulose matrix with HA particles were osteoconductive because 70% of the micro pores were smaller than 100 μm and only 3% of the macro pores were larger than 200 μm. The pore size of 200 mm in the interconnected porosity also helped induce cell attachment. The micro and macro pore sizes are considered fundamental aspects of scaffold functionality. New bone tissue can be formed on the surface that is suitable for good cell adhesion and growth. The pore interconnectivity provides the cells with the necessary conditions for cell distribution and migration, as well as the formation of blood vessels and the possibility of remodeling the bone tissue in the future.

Spherical HA particles were observed on the surface of the scaffolds, and at high magnifications each image revealed the formation of crystalline aggregates with a typical cauliflower-like morphology in the HA phase (Fig. 1) [44,45]. Theories on the HA formation process in calcium phosphates are the subject of debate. Bohner and Lemaitre [46] explained that HA has different growth strategies: (i) providing apatite nuclei, which eliminates the need for apatite crystal nucleation, (ii) providing a surface with low interfacial energy with apatite, or (iii) changing the local supersaturation towards apatite precipitation. The first strategy explains why HA is rapidly covered with the new apatite crystals, the second strategy provides an explanation for the formation of apatite on the β-TCP surface, and the third strategy elucidates why bioglass and other materials, such as calcium sulfate hemihydrate (CSH), are rapidly covered by an apatite layer upon immersion in SBF. Kim et al. [47] stated that the process of the bone-like apatite formation on sintered HA in SBF can be defined in 3 steps, as follows: the first structural change in the surface of the HA immersed in SBF came about through the formation of a Ca-rich ACP (amorphous calcium phosphate) on its surface, by means of the interaction with the positive calcium ions in the fluid. The second structural change in the surface was the formation of Ca-poor ACP, in which Ca-rich ACP with a positive surface charge interacting with the negative phosphate ions in the fluid. The third structural change in the surface was the formation of apatite, with the Ca-poor ACP on the HA stabilized by being crystallized into bone-like apatite.

Regarding the FTIR and Raman results, hydroxyapatite is known to be the mineral phase of bone tissue, and it is substituted with carbonate groups. There are two types of carbonate substitution: (1) direct substitution of OH^- with CO_3^{2-} (A-Type substitution CO_3^{2-} « 2 OH^-) and (2) necessity after change compensation, PO_4^{3-} substituting a tetrahedral group with $(CO_3)^{2-}$ (B-type substitution). The characteristics of HA crystallinity, crystal symmetry, thermal stability, morphology, solubility, and the physical, chemical, and biological characteristics in the lattice parameters are dependent on the type of substitution [48]. The Ca/P ratio of the HA was determined at 1.8, which corresponds to carbonated hydroxyapatite. The HA Ca/P ratio can vary from 1.2 to 2, depending on the site of the bone tissue or the stoichiometric apatite [49].

The X-ray diffraction patterns showed various phases. Na_3PO_4 manifested due to the incorporation of Na^+ ions into the bioglass phase structure of the scaffold. The second phases, $CaZrO_3$ and ZrP_2O_7, resulted from the incorporation of the Zr^{4+} ion into the structure of the pyrophosphate phase ($P_2O_7^{4-}$), which has two equivalent P sites as explained by Birkedal et al. [50]: Zr interact with the phosphate groups of the P-O-P type, in which the zirconium atoms are octahedrally coordinated as the Zr-O type, causing the bonds between the phosphate ions and the Zr to interact and form the P-O-Zr bonds, mainly as a ZrP_2O_7 phase.

The study of osteoblasts' behavior on different zirconia surfaces tends to mimic the behavior of dental implants, which promote stability in implant treatments based on higher and better osseointegration. In this work, the analysis of cell proliferation was performed; by cell counts at three, seven, and 14 days, the surfaces evaluated. We observed that at 14 days, the cells had a greater cell proliferation in VZ1.0. This effect

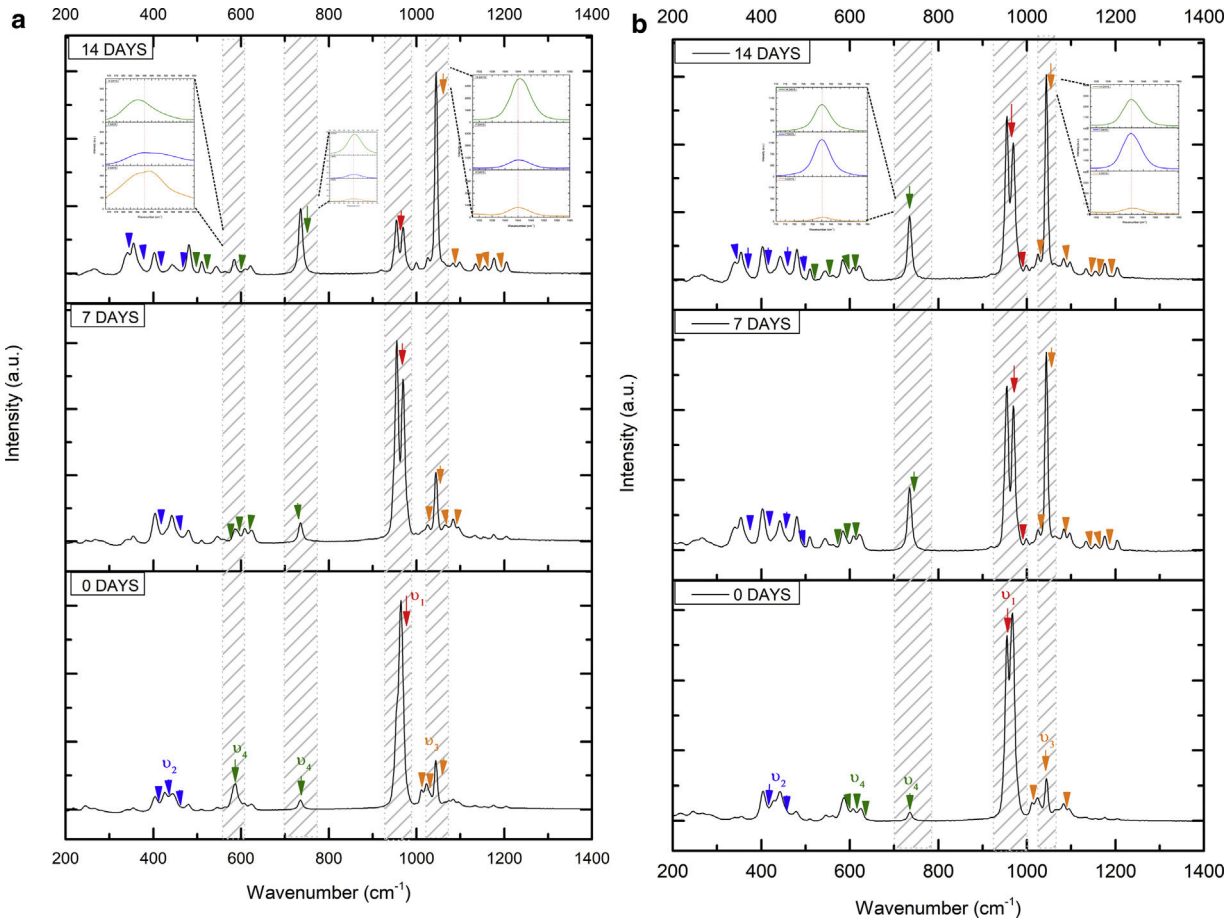

Fig. 8 – Raman spectrum of samples (a) VZ0.5 and (b) VZ1.0 after being immersed in SBF at different days (7 and 14 days).

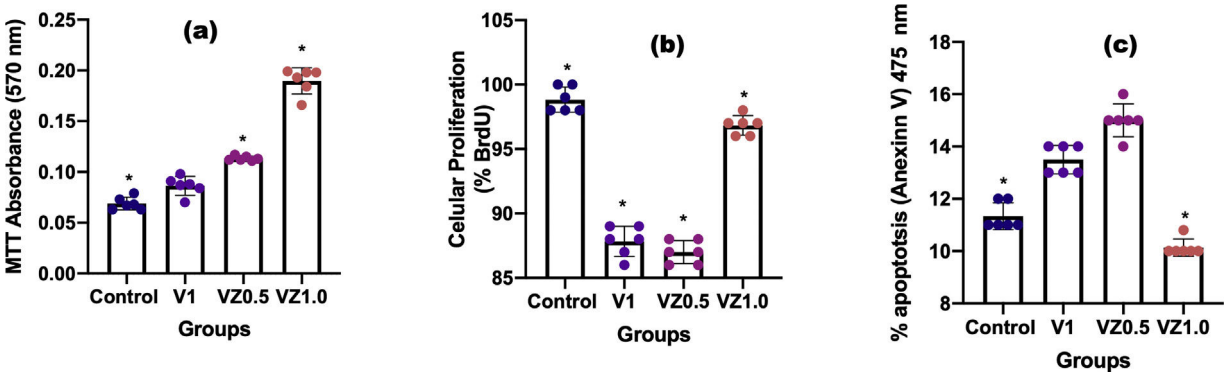

Fig. 9 – (a) MTT; (b) BrdU; (c) Anexinn V of the scaffolds V1, VZ0.5 and VZ1.0. The data are presented as mean ± standard deviation ($n = 3$) and the asterisks (*) indicate statistically significant difference ($p \leq 0.05$).

observed in all the culture periods, 3, 7, and 14 days. We also obtained a lower degree of cellular apoptosis in osteoblasts cultured on VZ1.0.

Furthermore, in those same discs (VZ1.0), the cultured osteoblasts presented more active mitochondria, showing a more active cellular energy state, by the MTT method. Acid-treated TZP surfaces have reported to demonstrate a significant increase in cell proliferation during the first days of culture but without strong surface adhesion. The latter does not agree with our data, since we found strong cellular adhesion, in VZ1.0, data that verified with the expression of the beta 3 integrin mRNA. Zirconia modified the scaffold surface, enabling better cell adhesion, a crucial step, and cell proliferation [51,52].

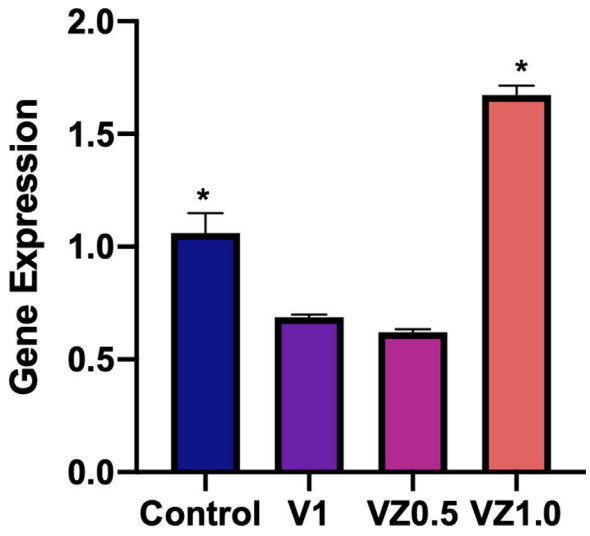

Fig. 10 – Gene expression of integrin β3 on osteoblast cells cultured on V1, VZ0.5 and VZ1.0. The data are presented as mean ± standard deviation ($n = 3$) and the asterisks (*) indicate statistically significant difference ($p \leq 0.05$).

Conclusions

In our research, we analyzed three different scaffold compositions of beta tricalcium phosphate/phosphate-based bioglass reinforced with zirconia (0, 0.5, and 1 mol.%). All three scaffolds, the so-called V1, VZ0.5, and VZ1.0, produced excellent results in relation to bioactivity in simulated body fluid and osteoconductivity in cell-culture media, with HA formation showed in both *in vitro* tests. Cells adhered well to scaffolds, especially VZ1.0 For all of the above, we conclude that the increase in surface porosity in the VZ1.0 biomaterial accelerates the proliferation, adhesion, and differentiation of osteoblastic cells, giving greater osteoinduction and osteoconduction.

Acknowledgements

The authors would like to acknowledge the CONACyT: Ciencia de Frontera "191982" to U.O.P and UNAM-DGAPA-PAPIIT: "IA105920" to U. O. P. for providing the funding for conducting this study.

REFERENCES

[1] Y. Kang, Y. Yao, G. Yin, Z. Huang, X. Liao, X. Xu, G. Zhao, A study on the in vitro degradation properties of poly(L-lactic acid)/beta-tricalcuim phosphate (PLLA/beta-TCP) scaffold under dynamic loading, Med. Eng. Phys. 31 (2009) 589–594.
[2] A. Marino, G. Rosso, F. Cafiero, G. Tortora, C. Moraci, M. Barbarisi, M. Barbarisi, β-Tricalcium phosphate 3D scaffold promotes alone osteogenic differentiation of human adipose stem cells: in vitro study, J. Mater. Sci. 21 (2010) 353–363.
[3] T. Lou, X. Wang, G. Song, Z. Gu, Z. Yang, Fabrication of PLLA/β-TCP nanocomposite scaffolds with hierarchical porosity for bone tissue engineering, Int. J. Biol. Macromol. 69C (2014) 464–470.
[4] J. Cai, S. Xu, H.G. Yu, Z.X. Zhang, Fabrication and biological characteristics of β-tricalcium phosphate porous ceramic scaffolds reinforced with calcium phosphate glass, J. Mater. Sci. 20 (2009) 351–358.
[5] F.H. Perera, F.J. Martínez-Vázquez, P. Miranda, A.L. Ortiz, A. Pajares, Clarifying the effect of sintering conditions on the microstructure and mechanical properties of β-tricalcium phosphate, Ceram. Int. 36 (2010) 1929–1935.
[6] K. Lin, L. Chen, H. Qu, J. Lu, J. Chang, Improvement of mechanical properties of macroporous β-tricalcium phosphate bioceramic scaffolds with uniform and interconnected pore structures, Ceram. Int. 37 (2011) 2397–2403.
[7] Y. Yang, Y. Zhao, G. Tang, H. Li, X. Yuan, Y. Fan, In vitro degradation of porous poly(l-lactide-co-glycolide)/β-tricalcium phosphate (PLGA/β-TCP) scaffolds under dynamic and static conditions, Polym. Degrad. Stab. 93 (2008) 1838–1845.
[8] H. Zhao, L. Ma, C. Gao, J. Wang, J. Shen, Fabrication and properties of injectable β-tricalcium phosphate particles/fibrin gel composite scaffolds for bone tissue engineering, Mater. Sci. Eng. C 29 (2009) 836–842.
[9] S.V. Dorozhkin, Bioceramics of calcium orthophosphates, Biomaterials 31 (2010) 1465–1485.
[10] G. Rajkumar, S. Aravindan, V. Rajendran, Structural analysis of zirconia-doped calcium phosphate glasses, J. NonCryst. Solids 356 (2010) 1432–1438.
[11] M. Bitar, V. Salih, V. Mudera, J.C. Knowles, M.P. Lewis, Soluble phosphate glasses: in vitro studies using human cells of hard and soft tissue origin, Biomaterials 25 (2004) 2283–2292.
[12] S.M. Rabiee, N. Nazparvar, M. Azizian, D. Vashaee, L. Tayebi, Effect of ion substitution on properties of bioactive glasses: a review, Ceram. Int. 41 (2015) 7241–7251.
[13] V. Salih, K. Franks, M. James, G.W. Hastings, J.C. Knowles, I. Olsen, Development of soluble glasses for biomedical use. Part II: The biological response of human osteoblast cell lines to phosphate-based soluble glasses, J. Mater. Sci. Mater. Med. 11 (2000) 615–620.
[14] M. Hisbergues, S. Vendeville, P. Vendeville, Review zirconia: established facts and perspectives for a biomaterial in dental implantology, J. Biomed. Mater. Res. B: Appl. Biomater. 88 (2008) 519–529.
[15] D. Bellucci, A. Sola, V. Cannillo, Bioactive glass-based composites for the production of dense sintered bodies and porous scaffolds, Mater. Sci. Eng. C: Mater. Biol. Appl. 33 (2013) 2138–2151.
[16] C.G. Jeong, S. Holliste Jr., Mechanical, permeability, and degradation properties of 3D designed poly(1,8 octanediol-co-citrate) scaffolds for soft tissue engineering, J. Biomed. Mater. Res. B: Appl. Biomater. 1 (2010) 141–149.
[17] C. Ruiz-Aguilar, E.A. Aguilar-Reyes, M. Flores-Martínez, C.A. León-Patiño, R.E. Núñez-Anita, Synthesis and characterization of β-TCP/bioglass/zirconia scaffolds, Adv. Appl. Ceram. 116 (2017) 452–461.
[18] E.A. Aguilar-Reyes, C.A. León-Patiño, B. Jacinto-Diaz, L.P. Lefebvre, Structural characterization and mechanical evaluation of bioactive glass 45S5 foams obtained by a powder technology approach, J. Am. Ceram. Soc. 95 (2012) 3776–3780.
[19] H.M. Kim, T. Himeno, M. Kawashita, T. Kokubo, T. Nakamura, The mechanism of biomineralization of bone-like apatite on synthetic hydroxyapatite: an in vitro assessment, J. R. Soc. Interface 1 (2004) 17–22.
[20] T. Kokubo, H. Takadama, How useful is SBF in predicting in vivo bone bioactivity? Biomaterials 15 (2006) 2907–2915.

[21] H. Tullberg-Reinert, G. Jundt, In situ measurement of collagen synthesis by human bone cells with a sirius red-based colorimetric microassay: effects of transforming growth factor β2 and ascorbic acid 2-phosphate, Histochem. Cell Biol. 112 (1999) 271–276.
[22] W. Hung, M. Shih, M. Hon, Wang., The properties of sintered calcium phosphate with [Ca]/[P] = 1.50, Int. J. Mol. Sci. 13 (2012) 13569–13586.
[23] A. Massita, Synthesis and characterization of nano-sized β-tricalcium phosphate: effects of the aging time, J. Appl. Chem. 7 (2014) 57–61.
[24] D.K. Pattanayak, R. Dash, R.C. Prasad, B.T. Rao, T.R.R. Mohan, Synthesis and sintered properties evaluation of calcium phosphate ceramics, Mater. Sci. Eng. C 27 (2007) 684–690.
[25] M.S. Maisara, M.L. Pat, K.H. Lee, Synthesis and characterization of hydroxyapatite nanoparticles and β-TCP particles, IPCBEE 7 (2011) 184–188.
[26] M. Fathi, A.E. Yacoubi, A. Massit, B.C. El, Idrissi, Wet chemical method for preparing high purity β-tricalcium-phosphate crystalline powders, IJSER 6 (2015) 139–143.
[27] E. Salimi, J. Javadpour, Synthesis and characterization of nanoporous monetite which can be applicable for drug carrier, J. Nanomater. 2012 (2012) 1–5.
[28] N.U. Kamrun, B. Shovon, C.D. Rajib, C.P. Shujit, B. Shukanta, Y.M. Muhammed, I.M.D. Sydul, Characterization of beta-tricalcium phosphate (β-TCP) produced at different process conditions, vol. 7, 2017, pp. 2–5.
[29] K. Agrawal, G. Singh, D. Puri, S. Prakash, Synthesis and characterization of hydroxyapatite powder by sol-gel method for biomedical application, JMMCE 10 (2011) 727–734.
[30] D. Bayraktar, A. Cu, È. Tas, Chemical preparation of carbonated calcium hydroxyapatite powders at 37 C in urea-containing synthetic body fluids, J. Eur. Ceram. Soc. 19 (1999) 2573–2579.
[31] J.D.S. Rabelo, T. Balesteri, M.C. Fredel, S. Olate, P.H. De, Moraes, Synthesis and characterization of calcium phosphate compounds with strontium and magnesium ionic substitutions, Int. J. Morphol. 33 (2015) 1189–1193.
[32] J. Ni, M. Wang, In vitro evaluation of hydroxyapatite reinforced polyhydroxybutyrate composite, Mater. Sci. Eng. C 20 (2002) 101–109.
[33] P.N. Chavan, M.M. Bahir, R.U. Mene, M.P. Mahabole, R.S. Khairnar, Study of nanobiomaterial hydroxyapatite in simulated body fluid: formation and growth of apatite, Mater. Sci. Eng. B 168 (2010) 224–230.
[34] G.M. Oliveira, M.P. Ferraz, P.G. González, J. Serra, B. Leon, M. Pérez-Amor, F.J. Monteiro, PLD bioactive ceramic films: the influence of $CaO–P_2O_5$ glass additions to hydroxyapatite on the proliferation and morphology of osteblastic like-cells, J. Mater. Sci. Mater. Med. 19 (2008) 1775–1785.
[35] H. Kienapfel, C. Sprey, A. Wilke, P. Griss, Implant fixation by bone ingrowth, J. Arthroplasty 14 (1999) 355–368.
[36] X. Lu, Y. Leng, Theoretical analysis of calcium phosphate precipitation in simulated body fluid, Biomaterials 26 (2005) 1097–1108.
[37] I. De Fátima Gimenez, I.O. Mazali, O.L. Alves, Application of Raman spectroscopy to the study ofthe phase composition of phosphate based glass-ceramic, J. Phys. Chem. Solids 62 (2001) 1251–1255.
[38] F.J. Buchanan, Bioresorbable ceramics. Degradation Rate of Bioresorbable Materials: Prediction and Evaluation, Woodhead Publishing series in Biomaterials, Elsevier, 2008, pp. 1–424.
[39] G. Penel, C. Delfosse, M. Descamps, G. Leroy, Composition of bone and apatitic biomaterials as revealed by intravital Raman microspectroscopy, Bone 36 (2005) 893–901.
[40] V.V.A. Nosenko, M. Yaremko, V.M. Dzhagan, I.P. Vorona, Y.A. Romanyuk, I.V. Zatovsky, Nature of some features in Raman spectra of hydroxyapatite-containing materials, J. Raman Spectrosc. 47 (2016) 726–730.
[41] M. Kazanci, P. Fratzl, K. Klaushofer, E.P. Paschalis, Complementary Information on In Vitro Conversion of Amorphous (Precursor) Calcium Phosphate to Hydroxyapatite from Raman Microspectroscopy and Wide-Angle X-Ray Scattering, vol. 79, 2006, pp. 354–359.
[42] D.L. Goloshchapov, A.S. Lenshin, D.V. Savchenko, P.V. Seredin, Importance of defect nanocrystalline calcium hydroxyapatite characteristics for developing the dental biomimetic composites, Results Phys. 13 (2019) 1–8.
[43] M. Mastrogiacomo, S. Scaglione, R. Martinetti, L. Dolcini, F. Beltrame, R. Cancedda, R. Quarto, Role of scaffold internal structure on in vivo bone formation in macroporous calcium phosphate bioceramics, Biomaterials 27 (2006) 3230–3237.
[44] H. Deplaine, M. Lebourg, P. Ripalda, A. Vidaurre, P. Sanz-Ramos, G. Mora, F. Prósper, I. Ochoa, M. Doblaré, J.L. Gómez Ribelles, I. Izal-Azcarate, G. Gallego, Ferrer, Biomimetic hydroxyapatite coating on pore walls improves osteointegration of poly (L-lactic acid) scaffolds, J. Biomed. Mater. Res. B: Appl. Biomater. 101 (2013) 173–186.
[45] K. Rezwan, Q.Z. Chen, J.J. Blaker, A.R. Bocaccini, Biodegradable and bioactive porous polymer/Inorganic composite scaffolds for bone tissue engineering, Biomaterials 27 (2014) 3413–3431.
[46] M. Bohner, J. Lemaitre, Can bioactivity be tested in vitro with SBF solution? Biomaterials 30 (2009) 2175–2179.
[47] H.M. Kim, T. Himeno, T. Kokubo, T. Nakamura, Process and kinetics of bonelike apatite formation on sintered hydroxyapatite in a simulated body fluid, Biomaterials 26 (2005) 4366–4373.
[48] L. Berzina-Cimdina, N. Borodajenko, Research of calcium phosphates using fourier transform infrared spectroscopy – Materials Science, Engineering and Technology, Prof. Therophanides Theophile Rijeka Croatia (2012).
[49] P.L. Stanciu, G.A. Sandulescu, B. Savu, S.G. Stanciu, K.M. Paraskevopoulos, X. Chatzistavrou, E. Kontonasaki, Investigation of the Hydroxiapatite growth on bioactive glass surface, J. Biomed. Pharm. Eng. 1 (2007) 34–39.
[50] H. Birkedal, A.M.K. Andersen, A. Arakcheeva, G. Chapuis, P. Norby, P. Pattison, The room-temperature superstructure of ZrP_2O_7 is orthorhombic: there are no unusual 180 degrees P—O—P bond angles, Inorg. Chem. 45 (2006) 4346–4351.
[51] R. Depprich, M. Ommerborn, H. Zipprich, C. Naujoks, J. Handschel, H.P. Wiesmann, N.R. Kübler, U. Meyer, Behavior of osteoblastic cells cultured on titanium and structured zirconia surfaces, Head Face Med. 4 (2008) 1–9.
[52] M.A. Fernández-Tresguerres Hernández-Gil, M. Alobera Garcia, L. Del Canto-Pingarrón, Blanco-Jerez, Physiological bases of bone regeneration I. Histology and physiology of bone tissue, Med. Oral Patol. Oral Cir. Bucal. 11 (2006) E47–E51.